https://doi.org/10.22226/2410-3535-2022-4-493-498

Strength and fracture mechanism of nanostructured metal materials for medical applications

G. V. Klevtsov[†,1], R. Z. Valiev[2], M. V. Fesenyuk[3], N. A. Klevtsova[1],
M. N. Tyurkov[1], A. A. Matchin[4], E. V. Nosov[4]

[†]Klevtsov11948@mail.ru

[1]Togliatti State University, Togliatti, 445020, Russia
[2]Ufa University of Science and Technology, Ufa, 450076, Russia
[3]JSC PA "Strela", Orenburg, 460005, Russia
[4]Orenburg State Medical University, Orenburg, 460000, Russia

In this paper we study titanium Grade4, magnesium alloy Mg-Zn-Ca, corrosion-resistant austenitic steel 08Kh18N9 for medical applications. The mechanical properties in tension, torsional strength, and cyclic crack resistance under different types of loading of steels are investigated. The results are compared for two states of steels: the initial coarse-grained (CG) state and ultrafine-grained (UFG) state produced by severe plastic deformation processing via equal-cannel angular pressing (ECAP). It is demonstrated that the ultrafine-grained materials have essentially better strength and lower sensitivity to cyclic overloads. It is concluded that all the studied UFG materials are more promising compared to CG ones for the manufacture of medical devices for various purposes, which experience various static and cyclic loads during operation.

Keywords: equal-cannel angular pressing, strength, fracture mechanism, materials for medical applications.

1. Introduction

Reducing the traumatism during surgery and period of postoperative rehabilitation in maxillofacial surgery, dentistry, traumatology and other fields of medicine involves the miniaturization of medical devices, for example, various implants, plates for bone osteosynthesis, rods and screws for the fixation of plates and bone fragments. During operation the products may experience various loads, both in terms of the amount and type of loading, static or cyclic [1,2]. Therefore, the task of miniaturization of medical devices cannot be solved without the use of materials that, in addition to good biocompatibility, have a high complex of mechanical properties under various types of loading [3–7]. These requirements are fully satisfied by a new class of bulk nanostructured metallic materials with an ultrafine-grained (UFG) structure produced by severe plastic deformation (SPD) processing [3,7,8–12]. Numerous studies indicate that the UFG structure formation significantly increases the hardness, strength, and fatigue limit of metallic materials [11–13] but reduces or slightly increases the fatigue strength in the region of low-cycle fatigue [9,14]. This fully applies to materials such as titanium, magnesium alloys and corrosion-resistant austenitic steels widely used in maxillofacial surgery, dentistry and traumatology [6,7,15–19].

The aim of the present study is to evaluate the strength and fracture mechanisms under static (tensile and torsion) and cyclic loading of UFG materials for medical applications in comparison with their coarse-grained (CG) counterparts.

2. Materials and methods

We selected titanium Grade4 (0.003% N; 0.008% C; 0.0006% H; 0.32% O; 0.38% Fe), magnesium alloy Mg-Zn-Ca (1.0% Zn, 0.2% Ca) and corrosion-resistant austenitic steel 08Kh18N9 (0.023% C; 17.95% Cr; 7.95% Ni; 1.85% Mn; 0.35% Mo; 0.38% Si; 0.6% Cu; 0.15% Co) widely used in medicine as the materials to be studied in the UFG and CG states.

Titanium Grade4 was studied in the initial CG state produced by homogenization annealing of hot-rolled billets at a temperature of 680°C for 1 hour. The UFG state of the billets was produced by equal-cannel angular pressing (ECAP) using two processing modes: 1) annealing + ECAP-conform (ECAP-C) at 250°C (route Bc, $\varphi=120°$, $n=6$) [10]; 2) annealing + ECAP-C at 200°C + drawing (D) at 200°C. Magnesium alloy Mg-Zn-Ca in the CG state was investigated after homogenization annealing at a temperature of 450°C for 24 hours followed by cooling in water. ECAP was carried out according to the following regime: route Bc, $\varphi=120°$, $n=2$ at a temperature of 430°C + $n=1$ at a temperature of 400°C + + $n=1$ at a temperature of 350°C.

Austenitic steel was investigated in the initial (hot-rolled) CG state and also in the UFG state. The UFG structure in the steel was obtained by quenching from a temperature of 1050°C with preliminary holding for 1 hour + ECAP at a temperature of 350°C (route Bc, $n=4$, $\varphi=120°$).

The CG structure was studied using metallographic microscopes GX50 (Olympus, Tokyo, Japan) and Axiovert 40 MAT (Carl Zeiss, Oberkochen, Germany). The fine structure of UFG materials was investigated using a JEM-6390

scanning electron microscope and also JEM-2100 transmission electron microscope (JEOL, Tokyo, Japan), and the accelerating voltage was 200 kV. The hardness tests were performed using a TH 300 hardness tester (Beijing TIME High Technology Ltd., Beijing, China). The static tension tests of the cylindrical specimens with a diameter 3 mm were carried out using an H50KT universal testing machine (Tinius Olsen, Redhill, UK). The grip movement rate was 5 mm/min. The static tension tests were performed in compliance with Russian standard 1497-84. The torsion tests of the cylindrical specimens were carried out at a temperature 20°C using KTC 403-20-0.5 testing system, in compliance with Russian standard 3565-80. The gauge diameter of titanium specimens was 3 mm, and the diameter of austenitic steel specimens was 10 mm. The length of all specimens was 100 mm. The mechanical properties of materials under torsion were calculated from the "torque vs twist angle" diagram [20].

The fatigue tests were conducted on prismatic specimens 10 mm in thickness, 15 mm in height, and 80 mm in length via three-point bending using an Instron 8802 testing system (High Wycombe, UK). The fatigue tests were carried out at a temperature 20°C with loading frequency of $\nu = 10$ Hz, the loading ratio of $R = 0.1$, and different values of load cycle stress.

3. Results and discussion

The average grain size and tensile mechanical properties of the studied materials are presented in Table 1. It can be seen that after ECAP processing, the hardness and tensile strength of titanium Grade4 and austenitic steel 08Kh18N9 increase, whereas the ductility decreases. After ECAP processing, the ductility of the magnesium alloy Mg-Zn-Ca increases by a factor of 2.5 compared to the cast homogenized state (Table 1).

The torsion tests of the specimens show (Fig. 1) that the torque corresponding to macroscopic yielding is higher for the UFG materials than for the CG materials. The maximum number of revolutions and twist angle of the specimens of UFG materials are lower than those of the CG specimens (Fig. 1). The ultimate torsional strength (τ_k) and torsional yield strength ($\tau_{0.3}$) of titanium and magnesium alloy Mg-Zn-Ca increase by factors of 1.1 and 1.3, respectively, as compared with the CG state, while the relative shear (g) decreases by factors of 1.3 and 1.8. The ultimate torsional strength (τ_k) and torsional yield strength ($\tau_{0.3}$) of the UFG austenitic steel 08Kh18N9 increase by factors of 1.3 and 1.8, respectively, as compared with CG steel, while the relative shear (g) decreases by a factor of 2.4 (Table 2).

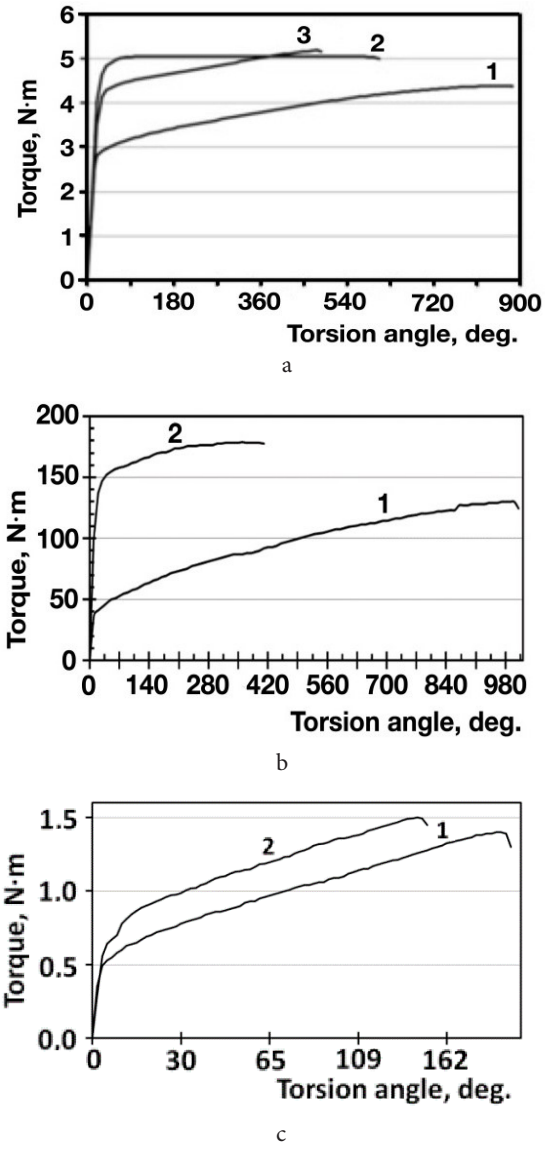

Fig. 1. "Torque-angle of twist" diagram based on the torsion tests of the specimens from the CG (1) and UFG (2, 3) titanium Grade4 (a): ECAP-C (2), ECAP-C + D (3), specimens from the CG (1) and UFG (2) corrosion-resistant austenitic steel 08Kh18N9 (b) and specimens from magnesium alloy Mg-Zn-Ca (c) in the initial state (1) and after ECAP (2).

Thus, it can be seen that UFG materials have a better resistance to torsional fracture than the materials in the CG state. This is a favorable factor that reduces the probability of fracture, for example, when unscrewing screws fused with bone during osteosynthesis of bones, since high values of the torsion strength properties of UFG materials make it possible

Table 1. Mean grain size (d_{mean}) and tensile mechanical properties of materials.

Material	State	d_{mean}, μm	HB	$\sigma_в$, MPa	$\sigma_{0.2}$, MPa	δ, %
Titanium Grade4	CG (annealing)	25	255	750 ± 10	650 ± 30	20 ± 0.5
	UFG (ECAP-C)	0.4	293	1050 ± 15	900 ± 25	14 ± 0.7
	UFG (ECAP-C +D)	0.2	-	1250 ± 10	1100 ± 30	11 ± 0.5
Magnesium alloy Mg-Zn-Ca	CG (anneling)	415	-	119 ± 9	65 ± 5	9 ± 0.3
	After ECAP	5÷40	-	210 ± 10	97 ± 7	23 ± 0.5
Corrosion-resistant austenitic steel 08Kh18N9	CG (initial)	30	159	624 ± 6	283 ± 2	65 ± 0.7
	UFG (ECAP)	0.55	363	1112 ± 15	1065 ± 15	20 ± 0.5

Table 2. Mechanical properties of the studied materials.

Material	∅, specimens, mm	State	τ_k, МПа	$\tau_{0.3}$, МПа	g, %
Titanium Grade4	3	CG (initial)	920 ± 37	641 ± 46	154 ± 3.5
		UFG (ECAP-C + D)	1014 ± 24	831 ± 18	87 ± 2.0
Magnesium alloy Mg-Zn-Ca	3	After annealing	264 ± 9	102 ± 5	33 ± 0.3
		After ECAP	283 ± 15	132 ± 10	25 ± 0.7
Corrosion-resistant austenitic steel 08Kh18N9	10	CG (initial)	688 ± 18	194 ± 11	89 ± 2.0
		UFG (ECAP)	917 ± 14	740 ± 12	37 ± 0.8

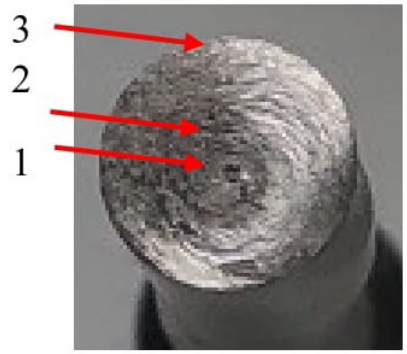

Fig. 2. Typical view of the fracture surface of the specimen during torsion: central part (1), transition (middle) part (2), and peripheral part (3).

to provide a high torque, and a low relative shear prevents the destruction of screws by shear.

Three regions can be distinguished in all the fracture surfaces: the ductile central part, the transition (middle) part, and the relatively smooth peripheral part (Fig. 2). The fracture surface microrelief reflects the process of fracture of the specimens during torsion. Fracture under torsional stresses of more plastic materials (titanium Grade4, corrosion-resistant austenitic steel 08Kh18N9) starts with the formation of shear dimples in the peripheral and middle regions of the fracture. The fracture of a more brittle magnesium alloy Mg-Zn-Ca begins with a cut in the peripheral region. With further torsion of the samples, formed shear dimples on the fracture surface of titanium and austenitic steel and sections of the cut on the fracture surface of the magnesium alloy turn out to be completely or partially rubbed out in the peripheral and transition regions (Fig. 3) as a result of mutual friction between the mating fracture surfaces. In the central part, fracture occurred under normal rupture stresses as evidenced by the predominantly equiaxed dimples on the fracture surface of titanium Grade4, and austenitic steel 08Kh18N9, and a mixed microrelief (tubular + dimples) in the fractures of the magnesium alloy Mg-Zn-Ca (Fig. 3).

At presents, to analyze a material's resistance to fatigue fracture in the low-cycle fatigue region, kinetic diagrams of fatigue fracture are used that describe the dependence of the fatigue crack propagation rate on the stress intensity coefficients ΔK or K_{max} [21].

Analysis of the rectilinear section of kinetic diagrams of fatigue fracture for the titanium Grade4 (Fig. 4a), and for the corrosion-resistant austenitic steel 08Kh18N9 (Fig. 4b) shows that at the same value of the coefficient ΔK, the fatigue crack propagation rates in the CG and UFG titanium Grade4 and in the CG and UFG corrosion-resistant austenitic steel 08Kh18N9 differ insignificantly. However, as it can be seen from Table 3, the coefficient n in the Paris equation for the UFG titanium and also for UFG corrosion-resistant austenitic steel is lower than that for the CG titanium and CG steel. Consequently, UFG titanium Grade4 and UFG corrosion-resistant austenitic steel 08Kh18N9 are sensitive to cyclic loads emerging during product operation as compared to the CG titanium and CG steel.

Let us consider the features of the fatigue failure mechanisms of titanium Grade4 and austenitic steel 08Kh18N9 in the CG and UFG states.

In the nucleation site of a fatigue crack in CG titanium, one can observe flat fragments (Fig. 5a) consisting of transcrystalline cleavage-like facets, the size of which approximately coincides with the grain size of CG titanium. At some distance from the crack initiation nucleus fatigue grooves and secondary cracks can be seen on the flat fragments (Fig. 5b). The final failure zone has a tubular microrelief; at the grain boundaries there are areas with a microrelief close to dimpled (Fig. 5c). The fatigue failure of the UFG titanium at all stages of fatigue crack propagation is characterized by the formation of a fine microrelief. At high magnification, ductile fatigue grooves and secondary cracks are visible (Fig. 5d, e). The final failure occurred by the quasi-cleavage mechanism with areas of dimpled microrelief (Fig. 5f).

The fatigue fractures of the CG steel 08Kh18N9 in the vicinity of the crack initiation nucleus have a microrelief oriented in the direction of the fatigue crack propagation (Fig. 6a). Ductile fatigue striations and secondary cracks parallel to them are visible at some distance from the crack initiation nucleus (Fig. 6b). The final failure zone of the CG steel has a dimple structure with deep, smooth dimples (Fig. 6c). In the fractures of the UFG steel ductile fatigue striations and secondary cracks can be observed already near the crack initiation nucleus (Fig. 6d). As the crack moves further, the secondary cracks on the fracture surfaces become larger and larger (Fig. 6e). The final failure zone of UFG steel consists of equiaxed deep dimples (Fig. 6f).

Tabl. 3. Paris equations.

Material	CG (Initial state)	UFG (ECAP)
Titanium Grade4	$\frac{dl}{dN} = 4.2 \cdot 10^{-15} (\Delta K)^{6.8}$	$\frac{dl}{dN} = 43 \cdot 10^{-13} (\Delta K)^{5.2}$
Austenitic steel 08Kh18N9	$\frac{dl}{dN} = 3.3 \cdot 10^{-15} (\Delta K)^{6.0}$	$\frac{dl}{dN} = 7.2 \cdot 10^{-12} (\Delta K)^{3.5}$

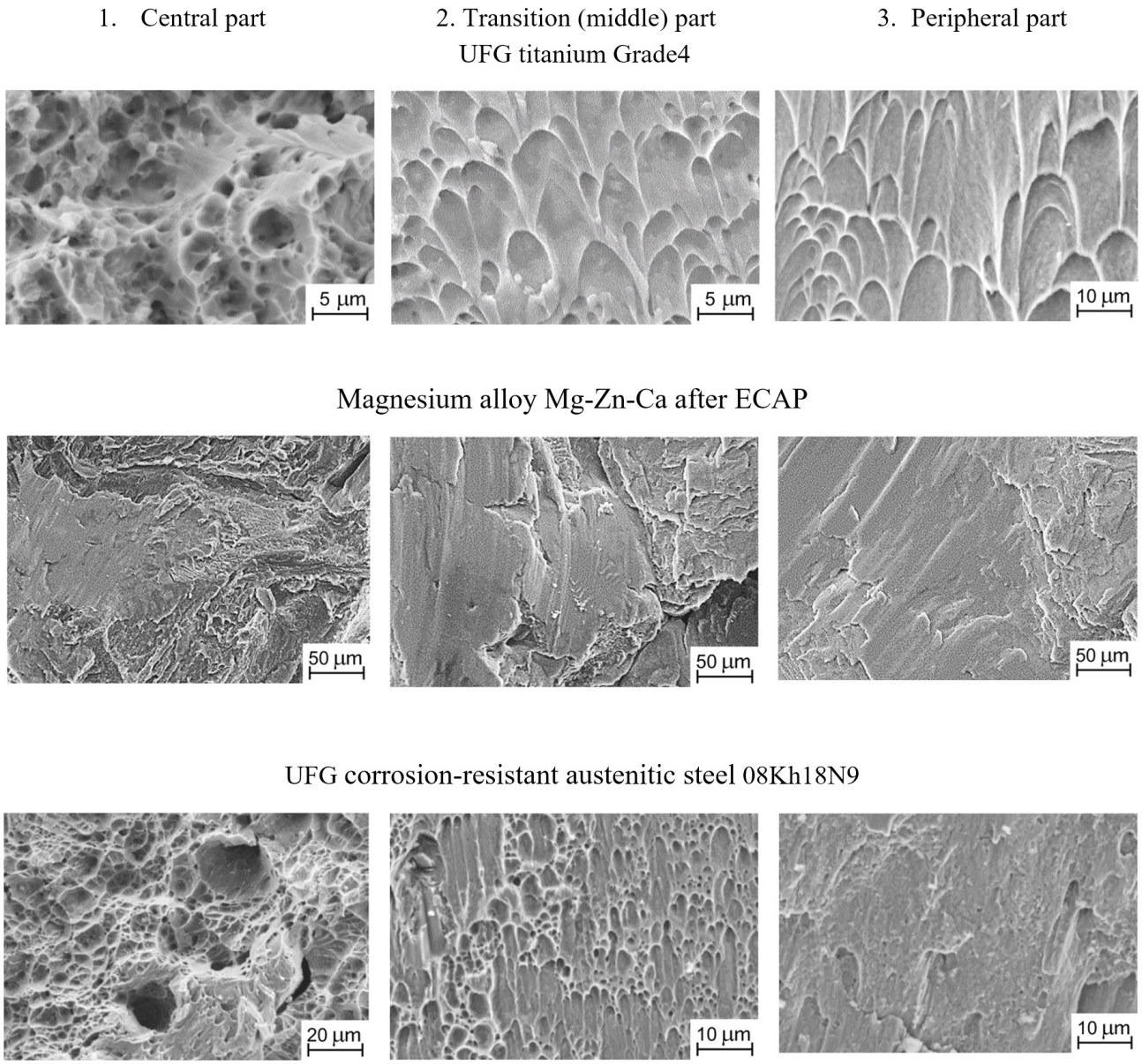

Fig. 3. Torsional fracture surface microrelief of the specimens after ECAP.

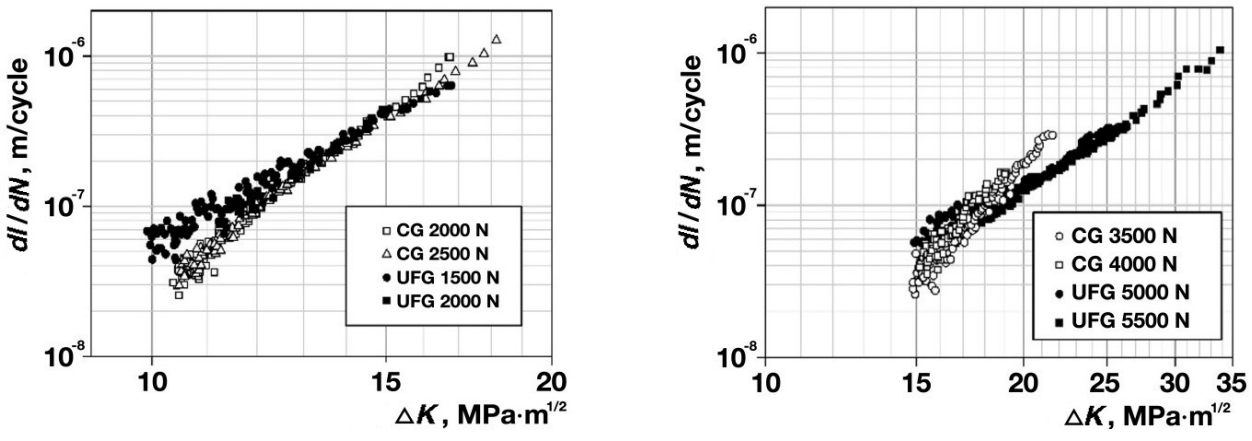

a b

Fig. 4. Straight-line portion of the kinetic diagrams of fatigue fracture for the titanium Grade4 (a) and the corrosion-resistant austenitic steel 08Kh18N9 (b). CG — bright dots, UFG — dark dots.

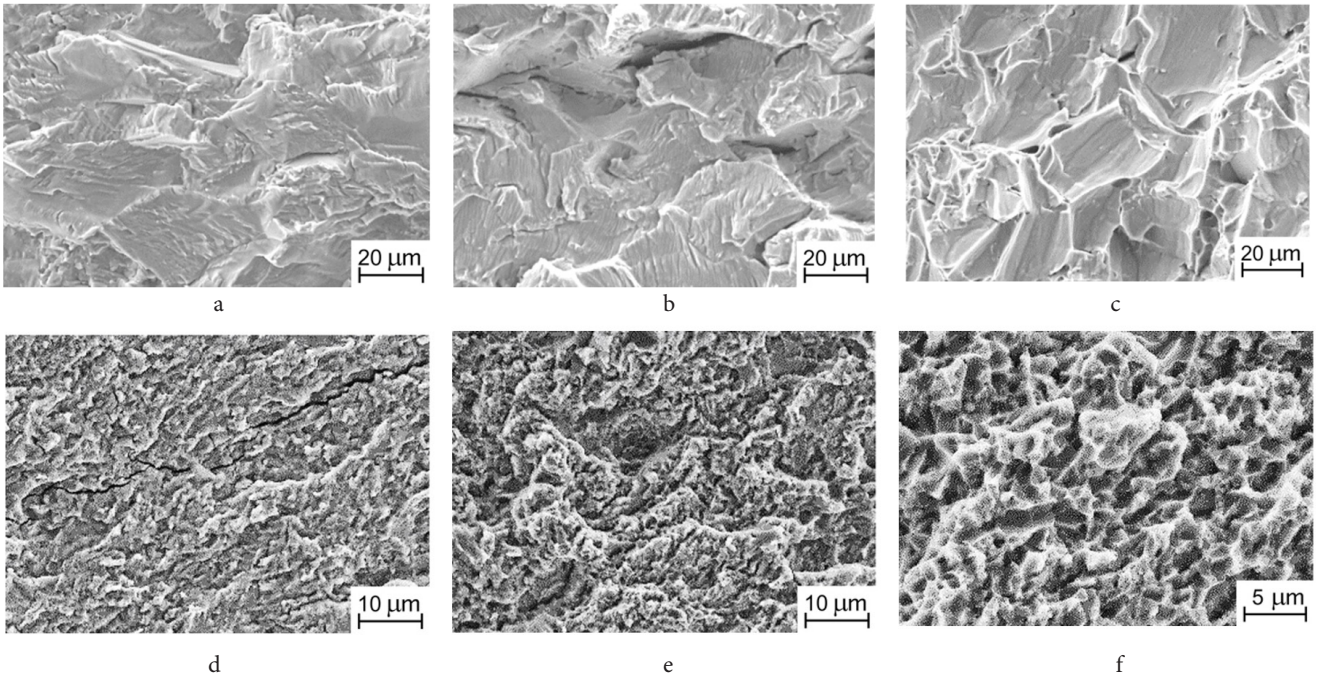

Fig. 5. Microrelief of the fatigue fracture surface of the CG (a – c) and UFG (d – f) titan Grade4 in the vicinity of the fracture nucleus (a, d), near the final failure zone (b, e) and in the final failure zone (c, f).

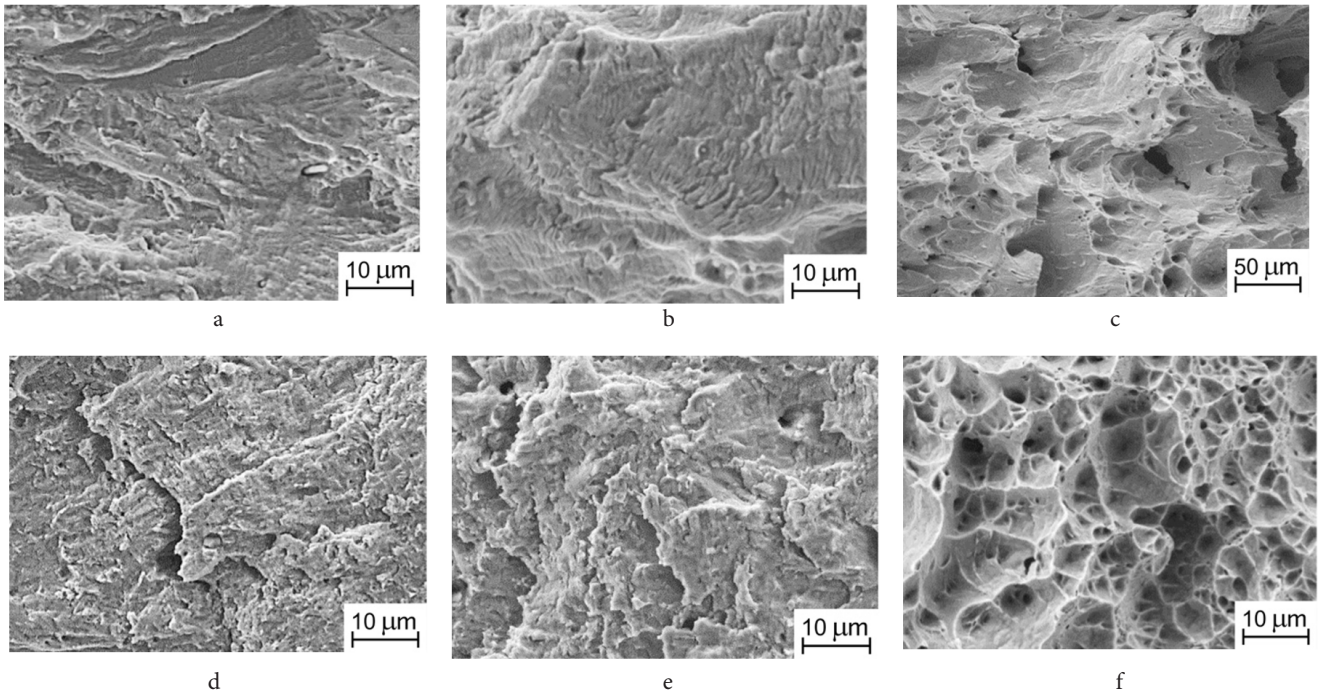

Fig. 6. Microrelief of the fatigue fracture surface of the CG (a – c) and UFG (d – f) steel 08Kh18N9 in the vicinity of the fracture nucleus (a, d), near the final failure zone (b, e) and in the final failure zone (c, f).

4. Conclusions

1. The equal-cannel angular pressing (ECAP) of the studied materials (titanium Grade4, magnesium alloy Mg-Zn-Ca and austenitic steel 08Kh18N9) provides an increase of hardness and strength properties, which will have a beneficial effect on the performance properties of medical products.

2. At the same value of the coefficient ΔK, the rates of propagation of a fatigue crack in CG and UFG titanium and steel differ insignificantly. However, the coefficient n in the Paris equations for UFG materials is lower than for materials in the CG state. Consequently, UFG materials are less sensitive to cyclic overloads that may occur during the operation of medical devices, compared to the CG state.

3. All studied UFG materials are more promising materials than their CG counterparts for the manufacture of medical products for various applications that experience various static and cyclic loads during operation.

Acknowledgements. This work was supported by a grant from the Russian Science Foundation (interdisciplinary projects no. 20-69-47059 and partially no. 20-63-47027). The authors thank TSU staff M.L. Linderov, I.N. Pigaleva and USATU staff G.I. Raab, A.V. Polyakov, M.M. Abramova, and O.B. Kulyasova for help in carrying out experimental studies.

References

1. J. S. Hayes, R. G. Richards. In: Encyclopedia of Biomedical Engineering (R. Narayan, ed. in Chief). Elsevier, Amsterdam, Netherlands (2019) pp. 257–269. Crossref
2. A.V. Popkov. The Genius of Orthopedics. 3, 94 (2014). (in Russian)
3. I.P. Semenova, G.N. Klevtsov, N.A. Klevtsova, G.S. Dyakonov, A.A. Matchin, R.Z. Valiev. Adv. Eng. Mater. 18, 1216 (2016). Crossref
4. R.Z. Valiev, I. Sabirov, E.G. Zemtsova, E.V. Parfenof, L. Dluhoš, T.C. Lowe. Woodhead Publishing, Duxford, UK (2018) 393 p. Crossref
5. T. Fujishiro, D.J. Moojen, N. Kobayashi, W.J. Dhert, T.W. Bauer. Clin. Orthop. Relat. Res. 469, 1127 (2011). Crossref
6. G.V. Klevtsov, R.Z. Valiev, N.A. Klevtsova, M.V. Fesenyuk, M.N. Tyurkov, A.V. Polyakov. Letters on Materials. 11 (3), 273 (2021). (in Russian) Crossref
7. G.V. Klevtsov, R.Z. Valiev, N.A. Klevtsova, M.N. Tyurkov, M.L. Linderov, M.M. Abramova, A.G. Raab, T.B. Minasov. Materials. 14, 7739 (2021). Crossref
8. Y. Estrin, A. Vinogradov. Acta Materialia. 61, 782 (2013). Crossref
9. Y. Estrin, A. Vinogradov. International Journal of Fatigue. 32, 898 (2010). Crossref
10. R.Z. Valiev, A.P. Zhilyaev, T.G. Langdon. Bulk Nanostructured Materials: Fundamentals and Applications. Hoboken, New Jersey, John Wiley & Sons (2014) 440 p. Crossref
11. I.A. Ovid'ko, R.Z. Valiev, Y.T. Zhu. Prog. Mater. Sci. 94, 462 (2018). Crossref
12. S.V. Dobatkin, W. Skrotzki, O.V. Rybalchenko, V.F. Terent'ev, A.N. Belyakov, D.V. Prosvirnin, G.I. Raab, E.V. Zolotarev. Mater. Sci.Eng. A. 723, 141 (2018). Crossref
13. I.A. Ovid'Ko, T.G. Langdon. Reviews on Advanced Materials Sci. 103 (30), 11 (2012).
14. A. Vinogradov, S. Nagasaki, V. Patland, K. Kitagawa, M. Kawazoe. Nanistruct. Mater. 11, 925 (1999). Crossref
15. I.P. Semenova, J.M. Modina, A.V. Polyakov, G.V. Klevtsov, N.A. Klevtsova, I.N. Pigaleva, R.Z. Valieva. Materials Science & Engineering A. 716, 260 (2018). Crossref
16. G.V. Klevtsov, R.Z. Valiev, M.V. Fesenyuk, N.A. Klevtsova, M.N. Tyur'kova, M.M. Abramova, G.I. Raab. Steel in Translation. 51 (11), 778 (2021). Crossref
17. G.V. Klevtsov, R.Z. Valiev, N.A. Klevtsova, M.V. Fesenyuk, O.B. Kulaysova, I.N. Pigaleva. Letters on Materials. 12 (3), 203 (2022). Crossref
18. A.A. Matchin, A.A. Stadnikov, E.V. Nosov, Klevtsov G.V. Journal of Medicine and Innovations. 1 (5), 123 (2022). (in Russian)
19. H. Mughrabi, H.W. Hoppel, M. Kautz. Scripta Materialia. 51, 807 (2004). Crossref
20. V.S. Zolotorevskiy. Mechanical properties of metals. Moscow, MISIS (1998) 400 p. (in Russian)
21. D. Broek Fundamentals of fracture mechanics. Moscow, Higher School (1980) 368 p. (in Russian)